

# Grain Boundary Versus Transgranular Ductile Failure in Aluminum Alloys

T. Pardoen<sup>1</sup>, D. Dumont<sup>2</sup>, A. Deschamps<sup>3</sup>, and Y. Brechet<sup>3</sup>

<sup>1</sup> Département des Sciences des Matériaux et des Procédés, Université catholique de Louvain, PCIM, Place Sainte Barbe 2, B-1348 Louvain-la-Neuve, Belgium

<sup>2</sup> Pechiney, Centre de Recherches de Voreppe, 725, rue Aristide Bergès, BP27, 38341 Voreppe, France

<sup>3</sup> LTPCM-ENSEEG, Domaine Universitaire de Grenoble BP75, F-38402 Saint Martin d'Herès, France.

**ABSTRACT:** *The competition between intergranular and intragranular fracture is investigated using a bilayer damage model, which incorporates the relevant microstructural features of aluminum alloys with precipitate free zones (PFZ) nearby the grain boundary. One layer represents the grain behavior: due to precipitation, it presents a high yield stress and low hardening exponent. The other layer represents the PFZ which has the behavior of a solid solution: much softer but with a much higher hardening capacity. In both layers, void growth and coalescence is modeled using an enhanced Gurson-type model incorporating the effects of the void aspect ratio and of the relative void spacing. Qualitative understanding of trends in the ductility fracture toughness of aluminum alloys can be gained in order to provide a link with the thermal treatment process.*

## INTRODUCTION

In aluminum alloys, appropriate heat treatment leads to fine precipitation which hardens the material. The yield stress first increases then decreases with the duration of the heat treatment. In parallel, the work hardening rate decreases when precipitation occurs. When the quench rate is slower, intergranular precipitation and coarse intragranular precipitation is more pronounced and the general effect is to lower the toughness. The generic evolution of the fracture toughness in a 7000-aluminum alloy is shown in Fig. 1. The failure mode is always ductile either intragranular or intergranular.

A schematics of the microstructure is shown in Fig. 2. The individual features controlling the fracture of 7000 alloys are identified. They indicate the relevant parameters to be introduced in our micromechanical model:

- The dispersoids particles provide sites for ductile cavity growth. These microstructural features are essentially controlled by the chemical composition

of the alloy, and are left unmodified by precipitation heat treatments. Therefore in the present approach, the number and initial size of cavities inside the grain will be considered constant.

- The influence of the heat treatments on the grain interior behaviour will be lumped into an evolution of the yield stress and work hardening behaviour. The typical behaviour of the grain interior after heat treatment will be a high yield stress  $\sigma_{0g}$  and a low work hardening rate  $n_g$ .
- The grain boundary microstructure classically exhibits a Precipitate Free Zone (PFZ) and grain boundary precipitates. The typical behaviour of the PFZ/grain boundary after heat treatment will be a low yield stress  $\sigma_{0p}$  and a high work hardening rate  $n_p$ .

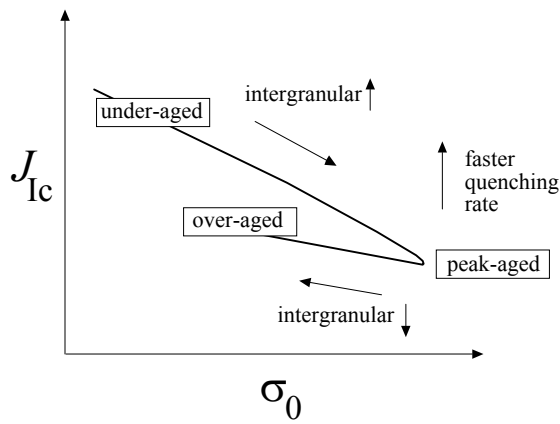


**Figure 1:** Effect of the aging treatment and quenching rate on the fracture toughness in 7000 aluminum alloys.

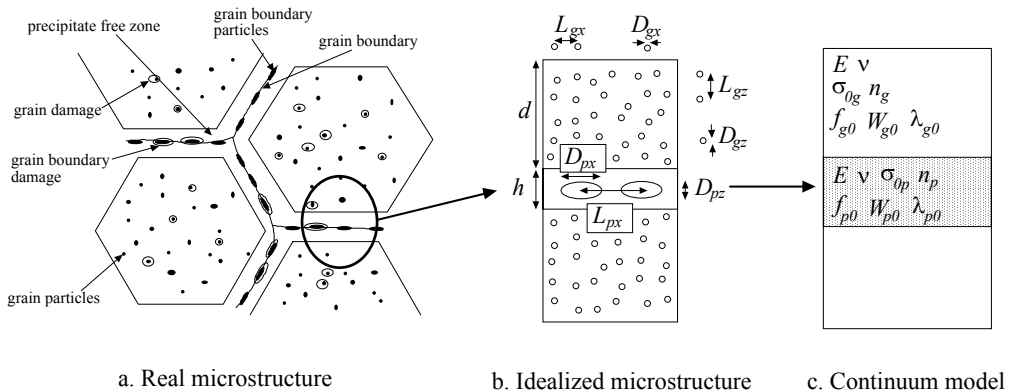


**Figure 2:** Description of (a) the microstructure and failure mechanisms, of (b) the idealized microstructure and of (c) the continuum micromechanical model. The parameters appearing in (b) and (c) are defined in Table 1.

The idealized microstructure is shown in Figure 2b. The length scales entering the problem are the grain size, the PFZ width, the size and spacing of intergranular precipitates (assumed to control the initial size and spacing of grain boundary nucleated cavities), the size and spacing of intragranular dispersoids (controlling the size and spacing of cavities within grains).

The uniaxial elastic and plastic tensile properties for the material in the grain interior and the PFZ interior are given by a simple two parameters description:

$$\frac{\sigma}{\sigma_0} = \frac{E\varepsilon}{\sigma_0} \quad \text{when } \sigma < \sigma_0, \quad (1)$$

$$\frac{\sigma}{\sigma_0} = \left( 1 + \frac{E\varepsilon^p}{\sigma_0} \right)^n \quad \text{when } \sigma > \sigma_0. \quad (2)$$

The modulus  $E$  is the same for the PFZ and the grain interior. The values of the parameters  $\sigma_0$  (yield stress) and  $n$  (hardening exponent) are given with a subscript "g" (resp. "p") for the grain interior (resp. for the PFZ).

The competition between intergranular and transgranular failure can be qualitatively understood in the following way (see Fig. 3). The PFZ is soft and is thus the first to deform plastically. The elastic grain imposes a strong constraint on the PFZ involving a large stress triaxiality. The large void growth rate in the PFZ lead to rapid coalescence of the voids. However, in some circumstances, the stress in the grain reaches the yield stress before the onset of coalescence in the PFZ, the stress triaxiality then drops in the PFZ which, due to its higher hardening capacity, now induces a higher constraint within the grain. Voids then tend to grow more rapidly within the grain. Due to the low hardening capacity of the grain, a state of damage induced softening is rapidly attained until voids finally coalesce within the grain.

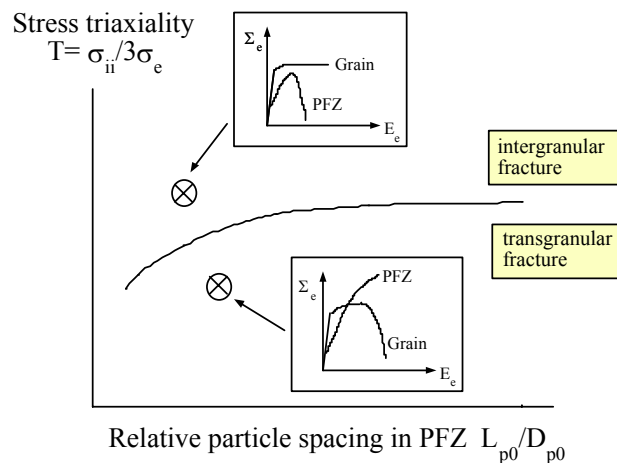


**Figure 3:** Failure map providing a qualitative understanding of the competition between intergranular and transgranular ductile failure.

A quantitative analysis of this highly non-linear problem of failure mode transition requires a detailed model for void growth and coalescence to be incorporated in each layer. The purpose of the present work was to use such a model in order to address the effect of the different microstructural characteristics on the transition between inter- and transgranular failure (given in terms of fracture mechanism maps as in Fig. 3). As the deformation process involves significant changes of stress triaxiality from very low to very high, the void growth model should be able to encompass large range of stress triaxiality.

### CONSTITUTIVE MODEL FOR BILAYER ELASTOPLASTIC MATERIALS WITH DUCTILE DAMAGE

The PFZ and the grain interior will be modeled using the same void growth and coalescence constitutive model, accounting for the different uniaxial flow properties and microstructure. Only the ingredients of the model are introduced in this section. Details can be found in Ref. [1].

- The model neglects the void nucleation phase as well as the presence of the precipitate within the void.
- The extension of the Gurson model [2] due to Gologanu *et al.* [3], which has been adopted here to describe behavior during void growth, gives a constitutive relation for a porous elastoplastic material containing spheroidal voids. This particular model, extended for strain-hardening in [1], contains as state variables: the components of the mesoscopic stress tensor,  $\Sigma$ , the porosity,  $f$ , the void aspect ratio,  $W$ , and an average yield stress for the matrix material,  $\sigma_y$ .
- Thomason [4] has studied the transition to localization for elastic-perfectly plastic solids by looking at artificially constrained localized solutions giving the load as a function of the void cell geometry. In Ref. [1], the Thomason analysis has been extended in order to derive a full constitutive model for the coalescence stage with additional equations for the evolution of the state variables during the post-localization stage.

The axisymmetric bilayer model is described in Fig. 2c. The two material layers are given the constitutive model described above. For the purpose of this work, the bilayer is deformed under constant imposed stress triaxiality. The symbols "g", "p" and "b" are used for quantities belonging to the "grain", to the "PFZ", and to the "bilayer" respectively. The basic relationships among the stress and strain rates components are the following :

$$\dot{\Sigma}_z^b = \dot{\Sigma}_z^g = \dot{\Sigma}_z^p, \quad (3)$$

$$\dot{E}_x^b = \dot{E}_x^g = \dot{E}_x^p, \quad (4)$$

$$\dot{E}_z^b = c\dot{E}_z^g + (1-c)\dot{E}_z^p, \quad (5)$$

$$\dot{\Sigma}_x^b = c\dot{\Sigma}_x^g + (1-c)\dot{\Sigma}_x^p + c(\dot{\Sigma}_x^g - \dot{\Sigma}_x^p)(\dot{E}_z^p - \dot{E}_z^b), \quad (6)$$

$$\dot{\Sigma}_z^b = \rho\dot{\Sigma}_x^b, \quad (7)$$

$$\begin{cases} \dot{\Sigma}_x^{p\ or\ g} = 2L_1^{p\ or\ g}\dot{E}_x^{p\ or\ g} + L_2^{p\ or\ g}\dot{E}_z^{p\ or\ g} \\ \dot{\Sigma}_z^{p\ or\ g} = 2L_3^{p\ or\ g}\dot{E}_x^{p\ or\ g} + L_4^{p\ or\ g}\dot{E}_z^{p\ or\ g} \end{cases}, \quad (8)$$

where  $\rho$  is the constant imposed stress ratio  $\Sigma_z/\Sigma_x$  (related to the stress triaxiality by  $\rho=(2+3T)/(3T-1)$ ), and  $c$  is equal to  $d/(d+h)$ . As long as coalescence has not started in one of the layer, the  $L$ 's are the tangent moduli which can be derived after straightforward, but lengthy, developments from the void growth constitutive relationships. When coalescence has started in one of the layer, the other layer unloads elastically. To a very a good approximation, the bilayer is then undergoing a uniaxial mode of deformation. The bilayer damage model described in section 2.1 and 2.2 has been assessed through a comparison with finite element bilayer void cell calculations (see [5]).

The initial relative spacing between particle along the grain boundary,  $L_{p0}/D_{p0}$ , will be used to present and interpret the results instead of the volume fraction of particle in the PFZ  $f_{p0}$ .  $L_{p0}/D_{p0}$  is univocally related to the previously defined parameters describing the microstructure.

## RESULTS

*Effect of the PFZ flow properties on the failure mode.* The competition between hardening and void softening in the PFZ is primarily driven by the flow properties of the grain with respect to the flow properties of the PFZ. Fig. 4 presents failure maps for three different ratio of  $\sigma_{0g}/\sigma_{0p}$  with the hardening exponent of the PFZ  $n_p$  equal to 0.4. As expected, an increase of the grain yield stress promotes grain boundary failure. An increase of the PFZ strain hardening capacity has an effect similar to a decrease of  $\sigma_{0g}/\sigma_{0p}$ .

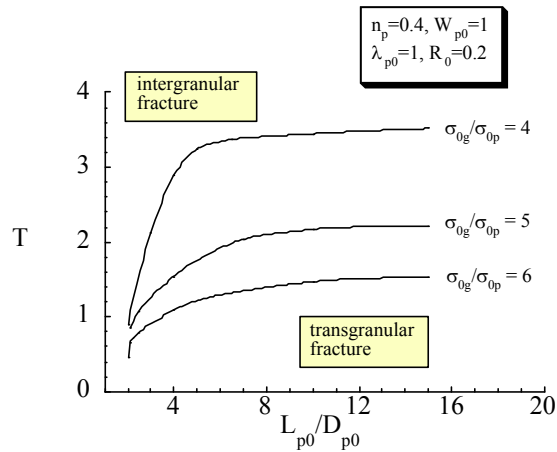


**Figure 4:** Effect of the yield stress ratio on the failure mode in a stress triaxiality versus relative particle spacing map.

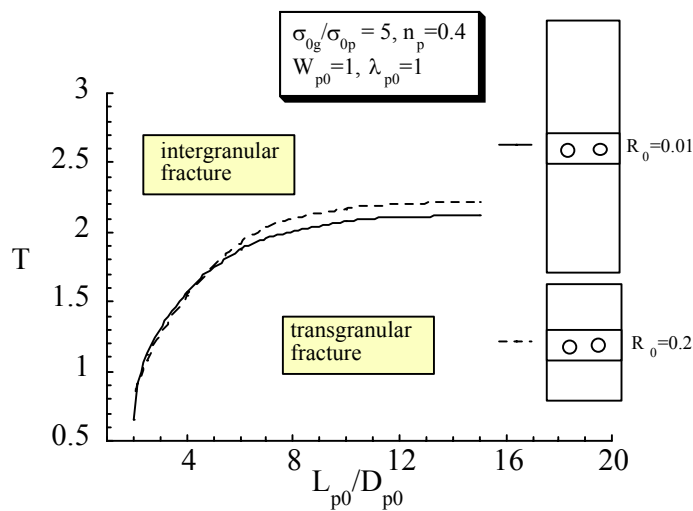


**Figure 5:** Effect of the PFZ thickness/grain size ratio on the failure mode in a stress triaxiality versus relative particle spacing map.

*Effect of the PFZ microstructure on the failure mode.* Calculations have been performed for two different PFZ relative thicknesses  $R_0$  equal to 0.01 and 0.2. Fig. 5 shows that the effect of  $R_0$  on the failure mode is marginal. The same conclusion is reached when looking at the effect of the initial void aspect ratio. The most important parameter, as exhibited in Fig. 6, is the spacing relative to the PFZ thickness,  $\sigma_{p0}$ .

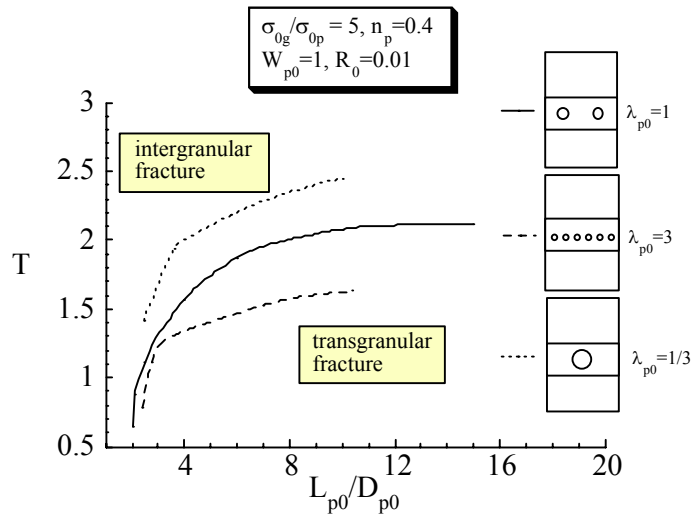


**Figure 6:** Effect of the PFZ thickness/void spacing ratio on the failure mode in a stress triaxiality versus relative particle spacing map.

The ductility is defined as the effective strain at final failure, i.e. at the end of the coalescence process. The triaxiality is prescribed by the external loading conditions. Figure 7 shows the variation of the ductility as a function of the stress triaxiality for  $R_0$  equal to 0.01 and 0.2. An exponential decay of the ductility as a function of the triaxiality is observed with a jump at the transition between transgranular and intergranular failure. It is interesting to note that  $R_0$  has a first order effect on the ductility and on the jump at the transition point.

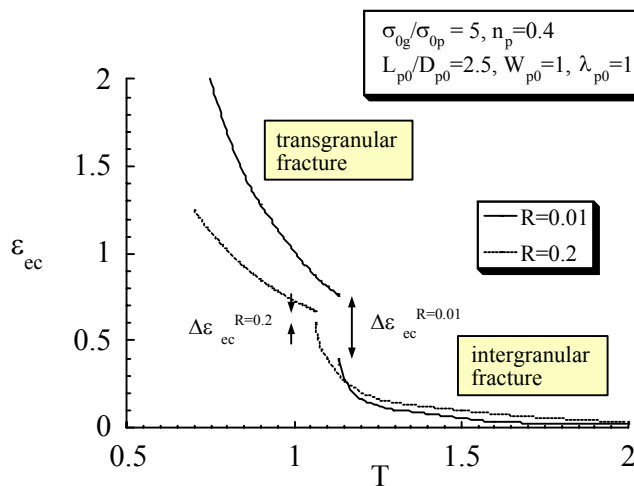


**Figure 7:** Variation of the ductility as a function of the stress triaxiality for two different relative PFZ thickness.

## DISCUSSION AND CONCLUSION

As already stressed, the model used in this work to address the competition between grain boundary ductile failure and transgranular ductile failure is not intended to give quantitative prediction of the ductility and of the exact locus of failure mode transition but to provide trends about the effect of the most relevant mechanical and microstructural parameters. (Considering the assumptions of the model: highly constrained bilayer geometry, no strain gradient effects, no account for cavitation instability).

The failure maps given in Fig. 4 to 6 show that, whatever the flow properties and microstructure, lower particle spacing  $L_{p0}/D_{p0}$  and high stress triaxiality always tend to promote intergranular fracture as expected from the qualitative description of Fig. 2. The stress triaxiality failure mode dependence has been qualitatively observed by D. Dumont [6]. Realistic values for  $L_{p0}/D_{p0}$  are between 2 and 5. In that range, the stress triaxiality corresponding with the failure mode transition is very much dependent on particle spacing which also complicates the optimization of the material properties.

The locus corresponding to the failure mode transition depends significantly on  $\sigma_{0g}/\sigma_{0p}$  and  $n_p$ . Simple estimates of the yield strength of solid solution and precipitation hardened materials has led us to estimate that  $\sigma_{0g}/\sigma_{0p}$  is equal or higher than 6 at the peak aging. The high sensibility of the transition to an intergranular failure mode on the grain strength has been observed by many investigators in both tension tests (low stress triaxiality) and fracture tests (high stress triaxiality), e.g. Dumont *et al.* [7]. It is much more difficult to both evaluate and modify the strain hardening capacity of the PFZ.

A change of  $R_0$  does almost not affect the failure mode transition locus when keeping all other parameters constant. This result agrees for instance with experimental measurements in systems where, using an interrupted quench, they were able to vary the width of a "vacancy depletion induced " PFZ without changing the grain boundary precipitation [8]. However, the value of  $R_0$  affects the ductility. Decreasing  $R_0$  implies an increasing constraint from the grain on the PFZ and thus a smaller ductility when fracture occurs at the grain boundary in agreement with Vasudevan and Doherty [9].

The most important microstructural feature that affects the failure mode is the PFZ thickness/void spacing ratio,  $\lambda_{p0}$ . Keeping  $L_{p0}/D_{p0}$  constant, a larger  $\lambda_{p0}$ , i.e. a larger PFZ, promotes earlier coalescence in the PFZ (see also [1] for a discussion about the effect of  $\lambda$ ) and, in the case of intergranular failure, significantly cuts down the ductility.

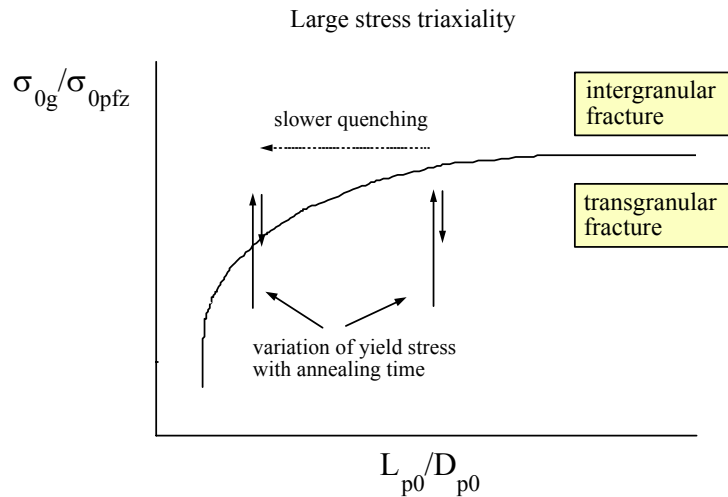


**Figure 8:** Schematic picture explaining the effect of the quenching rate and annealing time on the fracture toughness of 7000 Aluminum involving a competition between intergranular and transgranular failure.

In the experiments by David *et al.* [7], the increase of the grain yield stress is accompanied with an increasing proportion of grain boundary failure (see Fig. 1) and a much lower fracture toughness. Microstructural analysis have shown that decreasing quench rate lead to larger grain boundary particles and thus to lower relative particle spacing  $L_{p0}/D_{p0}$  value. These two effects can be understood using the results presented in this paper in terms of a  $\sigma_{0g}/\sigma_{0p}$  versus  $L_{p0}/D_{p0}$  map as proposed in Fig. 8 (high stress triaxiality). This map shows the locus for failure mode transition and gives a qualitative picture of the combined effect of the quench rate and aging time on the fracture toughness.

## REFERENCES

1. Pardoen, T. and Hutchinson, J.W., 2000. *Journal of the Mechanics and Physics of Solids* 48, 2467-2512.
2. Gurson, A.L., 1977. *Journal of Engineering Materials and Technology* 99, 2-15.
3. Gologanu, M., Leblond, J.-B., Perrin, G., and Devaux, J., 1995. Recent extensions of Gurson's model for porous ductile metals. *Continuum Micromechanics* (Edited by P. Suquet) Springer-Verlag.
4. Thomason, P.F., 1990. *Ductile Fracture of Metals*, Pergamon Press, Oxford.
5. Pardoen, T., Dumont, D., Deschamps, A., and Brechet, Y., 2002. Submitted for publication to the *Journal of the Mechanics and Physics of Solids*.

6. Dumont, D., 2001. *Relations Microstructure/Ténacité dans les Alliages Aéronautiques de la Série 7000*. Ph. D. Thesis, Institut National Polytechnique de Grenoble.
7. Dumont, D., Deschamps, A., and Brechet, Y., 2002. Submitted for publication to *Acta Materialia*.
8. Unwin, P. and Smith, G., 1969. *Journal of the Institute of Metals* 97, 299-310.
9. Vasudevan, A. and Doherty, R., 1987. *Acta Metallurgica* 35, 1193-1219.

#### **ACKNOWLEDGEMENTS**

The authors are grateful to Dave Embury, Jean Christophe Ehrstrohm, Eric Van der Giessen, and Patrick Onck for fruitful discussions. This work was partly carried out in the framework of program PAI 5-1-9 "*From microstructure towards plastic behaviour of single- and multiphase materials*" supported by SSTC, Belgium.